JET-P(95)09

The Physics of L and H Mode Confinement in JET

P Bak, B Balet, A Cherubini, J G Cordey, N Deliyanakis,
M Erba, V Parail, L Porte, E Springmann,
A Taroni, G Vayakis.

JET Joint Undertaking, Abingdon, Oxfordshire, OX14 3EA, UK.

Preprint of a paper to be submitted for publication in
Nuclear Fusion

July 1995

ABSTRACT

The results of numerical simulation of JET L, H and VH mode are presented. It is shown that L-H transitions are accompanied by a fast and large modification of the transport coefficients not only near plasma edge but across a large fraction of the plasma cross section. Both experiments and numerical simulations show that the giant ELMs on JET also have a global character, and their penetration length increases with the amplitude of the D signal. Transport coefficients are of the order of the L-mode ones during these ELMs. Analysis shows also that within experimental accuracy transport coefficients are the same for VH and ELM-free H-mode discharges. The variation in the global energy confinement is mainly due to the differences in the impurity radiation, power deposition profiles and the difference in the plasma recycling and related convection.

I. INTRODUCTION.

It has been shown [1], that all perpendicular transport coefficients (electron and ion thermal diffusivities χ_e and χ_i , plasma diffusion coefficient D and perpendicular viscosity μ) in JET drop over a very wide radial region ($0.5 \leq r/a \leq 1$) in a very sho A possible explanation is that plasma turbulence is correlated in radial direction by the plasma toroidicity [rt time scale ($\Delta\rho \leq 3$ms for χ_e) at the L-H transition. Fairly rapid changes in the electron temperature in the region 0.9>>0.7 have been also reported in the other tokamak experiments [2,3]. A possible explanation is that plasma turbulence is correlated in radial direction by the plasma toroidicity [4]. Therefore any modification of the anomalous transport coefficients (at L-H and H-L transitions and during ELMs) could propagate across the magnetic field with the group velocity of plasma turbulence (which is much faster than the velocity of heat pulse propagation). This idea has been tested by the numerical simulation of the evolution of plasma parameters during L-H transitions. Results of this analysis confirm the validity of this idea and allow us to develop a transport model which can describe the evolution of plasma parameters in L mode and throughout the L-H transition.

Our next step was an attempt to find whether substantially different transport is required to describe the evolution of local plasma parameters during the ELM-free H-mode phase in pulses which have different global energy confinement properties. It is known from transport analysis, that the global energy confinement time enhancement over its L-mode value can vary from $H \equiv \frac{\tau_E}{\tau_E^{ITER89}} \approx 2$ in ELM-free H-modes JET plasma up to $4.5 \geq H \geq 3$ in the VH mode phase. Such a wide range for the enhancement factor suggests that the transport properties of ELM-free H-mode plasmas could be quite different. On the other hand it also known that global energy confinement time is controlled not only by the local transport coefficients but also by

processes such as the shape of the power deposition profile, impurity radiation, plasma convection and large scale MHD processes. Last but not the least, another additional process which has a significant influence on plasma performance in the ELM-free H-mode is the appearance of the transport barrier near plasma edge which leads to the formation of the so called temperature (or density) pedestal. Analysis of experimental data shows that in the best JET hot ion H-mode shots almost half of the plasma energy is stored in such a pedestal. To analyse the relative importance of all these properties we chose several JET H-mode shots with enhancement factor in the range $2.5<H<4.5$ (including VH mode shots) and different plasma parameters and simulate them using the predictive transport code JETTO [5]. A Bohm type dependence on plasma parameters is used for the transport coefficients. Therefore the only possibile way to modify the transport properties was to vary the numerical factors in front of the transport coefficients. The basic result of this analysis is that within the experimental accuracy we can fit all selected shots with the same values of the numerical factors. Thus the main differences between regimes with very good confinement (VH modes with H3) and ELM-free H-mode with H3 lie not in transport properties.

As was mentioned above, one of the possible causes of difference in the global confinement might be a difference in the level of large scale MHD activity. The characteristic example of such macroscopic MHD instability are sawteeth or m=1, n=1 instability. Another interesting example observed in many tokamaks is the so called soft termination of the VH-mode (roll-over [6,7], or ETP [8]), which might be associated with MHD turbulence with larger m and n numbers (m>1, n1). The discussion of these events is outside the scope of our article.

The next cause of distinction between VH and ELM-free H-mode is the difference in power deposition profile [9] - generally speaking it is more peaked for VH modes. Finally there is an essential difference in the impurity radiation and in the level of convective losses. Both these effects can not directly influence plasma core confinement because both are localised near the plasma edge. Analysis shows however that these processes could significantly influence the magnitude of the temperature pedestal which provides an important input into the total energy content. To take these process properly into account we made use of boundary conditions which reproduce a neo-classical transport barrier, allowing us to predict the pedestal temperature.

The same approach is used for the numerical simulation of the giant ELMs. The idea was to find the radial distribution of enhanced transport and its temporal evolution during giant ELMs. The analysis shows that giant (type I in accordance with DIII-D classification) ELMs in JET also have a global character and can be modelled as a temporary transition into L mode triggered by a short MHD event. We managed to model this MHD event using an assumption that the electron thermal diffusivity is increased in the outer part of plasma column up to the level significantly larger than that of the L-mode one. This picture was also confirmed by recent

measurements of the evolution of the density fluctuations which show that the typical giant ELM on JET starts with a very short broad band burst of density fluctuations with characteristic duration time $\tau_{MHD} \approx 1ms$ This short burst is then followed by a much longer phase (with $\tau_L = 10-30ms$) of enhanced fluctuations with much narrower frequency band, which is typical of L-mode JET plasma.

The article is organised as follows. Section II is devoted to the description of the transport model for L and ELM-free H mode plasmas and possible ways to describe the formation of the temperature pedestal. In Section III we present the result of the numerical analysis of JET ELM-free H-mode shots with different enhancement factors. Section IV deals with the experimental observation of the density fluctuation during giant ELMs and with the numerical simulation of the evolution of the plasma parameters during giant ELMs. We summarise the main results in Section V.

II. TRANSPORT MODEL OF L-MODE AND ELM-FREE H-MODE JET DISCHARGES.

Our previous analysis showed [10] that the evolution of plasma parameters during the L-mode and shortly after L-H transition on JET could be well reproduced by Bohm-like coefficients for electron and ion thermal diffusivities:

$$\chi_e = \alpha_e \frac{c\left|\nabla(nT_e)\right|}{eBn} aq^2,\ \chi_i = \chi_i^{neo} + \alpha_i \frac{c\left|\nabla(nT_e)\right|}{eBn} aq^2 \qquad (1)$$

where χ_i^{neo} is the ion neo-classical thermal conductivity and the second term on the right hand side of χ_i and first in χ_e is an empirical Bohm-like coefficient, proposed and used in [11] to reproduce L-mode confinement in JET. We assume in (1) that q near the separatrix is limited by its $q_{\Psi=0.95}$ value. Note that the bohm-like coefficients in (1) which were used in our analysis are proportional to the pressure gradient. This leads to a certain amount of profile resiliency. It should therefore result in a faster then usual propagation of the heat pulse. Our analysis shows that we can reproduce the fast modification of electron temperature at the L-H transition only if we assume that both χ_e and χ_i are changed everywhere and not only near the separatrix. It was found that the best agreement with the old and new JET shots is achieved if we assume that the numerical coefficients α_e and α_i are reduced from:

$$\alpha_i^L \approx 3\alpha_e^L \approx 6 \cdot 10^{-4} \qquad (2)$$

in the L-mode to:

$$\alpha_i^H \approx 3\alpha_e^H \approx 0.6 \cdot 10^{-4} \qquad (3)$$

in the H-mode plasma [12]. Fig. 1 shows the radial distribution of χ_i and χ_i^{neo} for a typical L mode (# 19642, $P_{NBI}+P_{ICRH}=13MW$, $\bar{n}_e \approx 5.5\cdot 10^{19} m^{-3}$, $I_p=3MA$) and H mode (#32919, $P_{NBI}=17MW$, $\bar{n}_e \approx 4\cdot 10^{19} m^{-3}$, $B_T=3.4T$, $I_p=3MA$, $T_i(0)\approx 24keV$) plasma. It is worthwhile mentioning here that it follows from Fig.1 that neo-classical ion transport becomes important in the central part of plasma column during the H-mode phase.

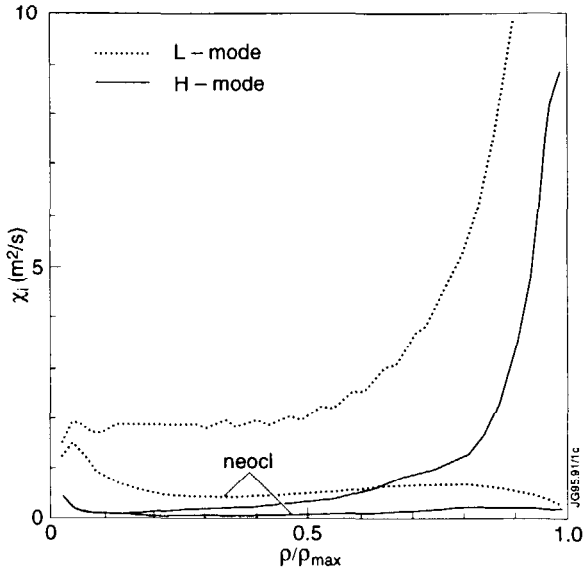

Fig.1: Neoclassical and total ion thermal diffusivity profiles from simulations of typical L-mode (#19642) and H-mode (#32919) JET discharges.

We assume that the same model could be used throughout the entire ELM-free H-mode phase for those shots which have no large scale MHD activity (sawteeth, ELMs, roll-over). To test the validity of this assumption we have selected a number of representative ELM-free H-mode discharges from the JET database and performed their numerical modelling with the predictive transport code JETTO. Some of the selected discharges fall into the category of VH mode with enhancement factor H>3 , while the others have 2≤H≤3. The main plasma parameters of the pulses are listed in Table 1.

Table I

Discharge	$<n_e>_{20}$	$<Z_{eff}>$	I_p (MA)	B_t (T)	P_{in} (MW)
25264	0.14→0.37	2.3	1.0	2.8	6.5
26087	0.19→0.30	1.6	3.2	2.8	15.0
26095	0.11→0.30	2.6	3.2	2.8	14.2
30591	0.15→0.36	2.5	2.4	2.7	15.0
30725	0.71→0.84	1.3	3.1	2.2	6.1
32919	0.12→0.43	2.2	3.0	3.4	18.0

The analysis was performed in the following way. All simulated pulses were analysed by TRANSP which provide both a consistency check of experimental data and the NBI power deposition profiles. The evolution of electron and ion densities has not been simulated, both density profiles and the profile of the radiated power being taken from experiment. We used the experimentally measured evolution of T_e and T_i near the separatrix as boundary conditions in our initial analysis. L-mode phases of all discharges were simulated with the same numerical coefficients α_e and α_i given by (2), ELM free H-mode with the coefficients given by (3). Note

that all shots from Table 1 but #30725 have features which could not be reproduced either by the L-mode or by the H-mode model. Namely shots ##26087, 30591 and 32919 had an ELMy H-mode phase during the initial phase of NBI heating. To model this phase we used halved L-mode transport coefficients (2). Shot #32919 had a slow roll-over during the interval 53.05s t 53.18s. To model this phase we used three times reduced L-mode transport coefficients (2).

III. NUMERICAL SIMULATION OF JET ELM-FREE H MODE PLASMA.

The temporal evolution of the measured thermal plasma energy content and that calculated with our model during the ELM-free H-mode phase for four discharges are shown in Fig.2. In Fig.3 experimental and simulated temperature profiles are compared.

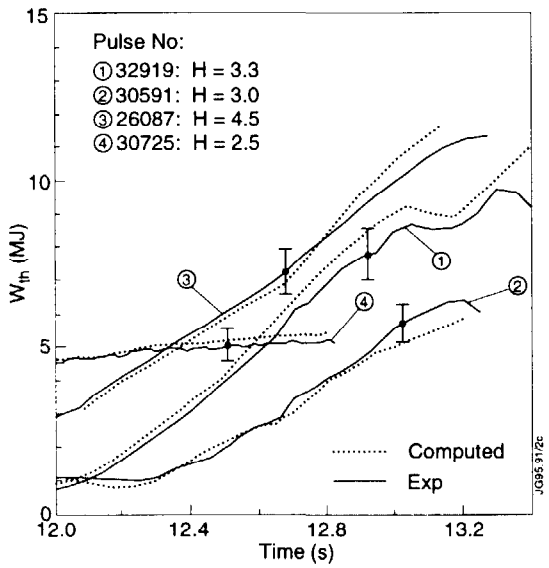

Fig.2: Time evolution of the thermal energy content given by TRANSP compared with the thermal energy predicted using the standard model for H-mode ELM-free JET discharges.

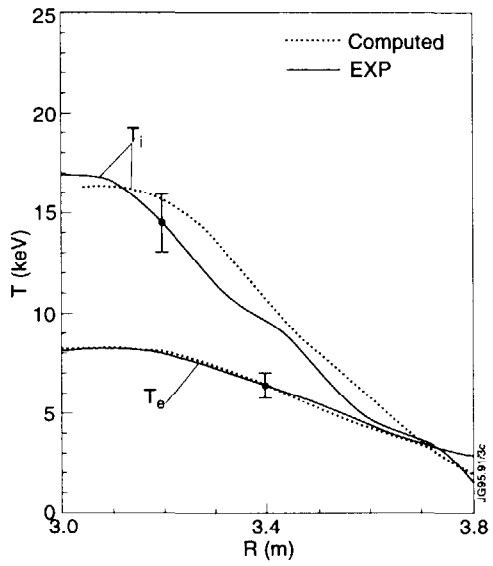

Fig.3: Experimental and computed ion and electron temperature profiles at the end of the H-mode ELM-free phase of discharge #30591.

We conclude that both the global features and the temperature profiles of apparently different ELM-free H-mode shots can be reproduced within the experimental accuracy by using transport coefficients as in Sec.II and prescribing experimental values for pedestal temperatures.

Therefore the transport coefficients in VH and other ELM-free H-mode with lower H factors are not radically different, and so they can not explain the difference in global confinement. This conclusion has been confirmed by TRANSP analysis. It was shown in particular that electron and ion thermal diffusivities are practically indistinguishable for the best hot-ion H-mode shots from the previous and the present experimental campaign everywhere apart from plasma edge, where however the interpretative analysis becomes inaccurate as a

result of plasma-wall interaction. Fig.4 shows the radial distribution of the effective thermal diffusivity computed by TRANSP for one of the best hot-ion H-mode from previous campaign #26087 and for the similar shot #30591 from the present campaign. On the other hand enhanced plasma-wall interaction may well be the cause of reduced energy confinement in the boundary region.

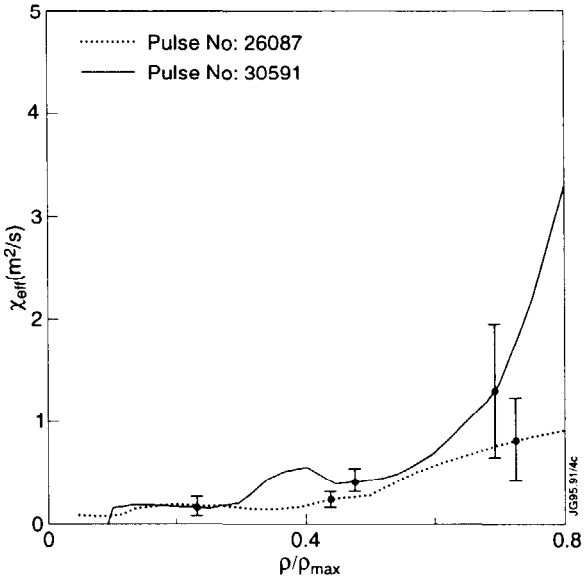

Fig.4: Effective heat diffusivity resulting from TRANSP analysis for the H-mode ELM-free phase of discharges #26087 and #30591.

It has been already mentioned that differences in power deposition profiles are one of the possible causes for changes in performance of NBI heated ELM-free H-modes. Numerical analysis shows that NB does not penetrate to the centre of the plasma in high density shots: Fig.5 shows ion power deposition profiles computed by TRANSP for shot #26087, with relatively low density, and shot #30725, with higher density. Broadened deposition profiles can lead to a deterioration in plasma performance. To illustrate this effect we compare in Fig.6 the temporal evolution of the thermal plasma energy content for shot #26087 computed with different deposition profiles but with the same transport coefficients and other plasma parameters.

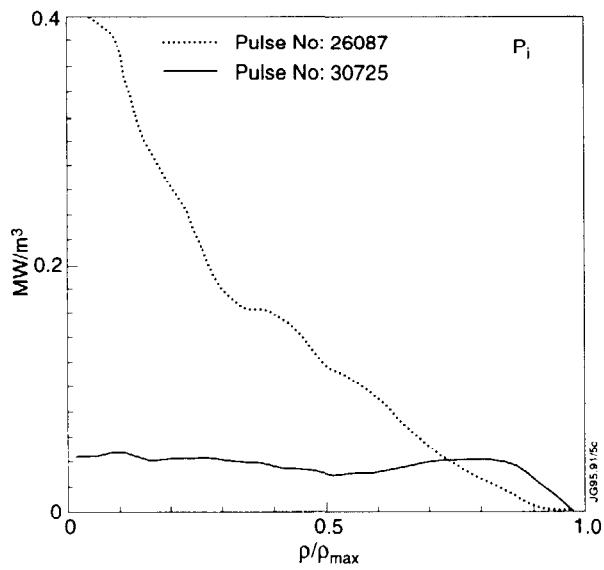

Fig.5: Ion power deposition profiles for shots #30725 and #26087.

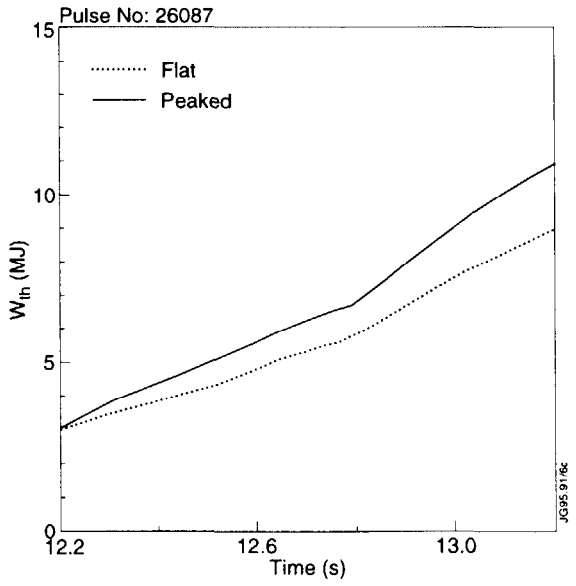

Fig.6: Time evolution oif the Thermal energy content of discharge #26087 computed using the peaked deposition profiles given by TRANSP for this case and flat deposition profiles given by TRANSP for discharge #30725.

The temperature pedestal is another important source of difference in plasma performance. To illustrate this point we define the energy stored in the temperature pedestal as: $W_{e,i}^{ped} = 3/2\langle n_{e,i}\rangle T_{e,i}^{edge} V$ where $<n>$ is the volume average density and V is the plasma volume. Fig.7 shows, for the two shots #26087 and #30725, the temporal evolution of the total W^{ped} together with the total thermal energy as computed by TRANSP.

Two interesting features are observed in shot #26087 which are typical for the best hot-ion VH mode JET shots:

- more than half of the thermal plasma energy is stored in the pedestal.

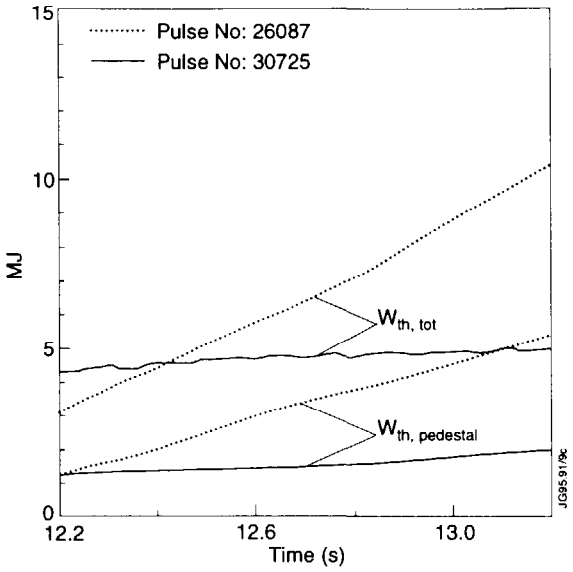

Fig.7: Time evolution of the thermal energy content given by TRANSP compared with the energy content of the temperature pedestal for shots #26087 and #30725.

- both total thermal energy content W_{th} and W^{ped} continuously grow in time and do not saturate during the heating. This leads to a continuous rise in both total and thermal energy confinement time, which maximum value is therefore controlled by different kind of MHD instabilities.

As was mentioned earlier, we did not simulate the temperature pedestal evolution in our previous analysis, instead we used the experimentally measured electron and ion temperature near the separatrix as a boundary condition. This allows us to disregard the physics of the temperature pedestal formation as well as such processes as impurity radiation and convective losses, which are both localised near the plasma edge and therefore influence plasma performance almost only through modification of the edge temperatures. But the cost of such a simplification is the lack of understanding of the importance of these processes and loss of predictability of the numerical simulation. Therefore we tried to find a self consistent way of simulating the temperature and density evolution near the separatrix. The problem is that the evolution of the plasma parameters in this region is controlled not only by the perpendicular transport processes inside the confined region but also by the longitudinal transport processes beyond the separatrix. The proper description of the transport in the SOL requires 2D modelling which is far outside the scope of this article. Instead we simplified the problem by integrating the transport equations across the SOL. These integrated equations can be used as boundary conditions for the main plasma:

$$\chi_{e,i} n_{e,i} \nabla T_{e,i} + \frac{3}{2} T_{e,i} D \nabla n_{e,i} \approx -\alpha_T \frac{\Delta}{L_{||}} c_{SOL} T_{e,i} n_{e,i} \quad (4)$$

$$D \nabla n_e \approx -\alpha_n \frac{\Delta}{L_{||}} c_{SOL} n_e \quad (5)$$

where we assume that the total heat flux in equations for T_e and T_i evolution in the confined region contains both conductive $Q_{i,e}^{cond} = -n_{i,e}\chi_{i,e}\nabla T_{i,e}$ and convective $Q_{i,e}^{cond} = -\frac{3}{2} T_{i,e} D \nabla n_{i,e}$ parts. In (4-5) $T_{e,i}$ and $n_{e,i}$ are plasma parameters at the separatrix, $\Delta \propto \sqrt{D L_{||}/c_{SOL}}$ is the characteristic width of the SOL, $L_{||}$– the longitudinal connection length of the SOL, c_{SOL}– the characteristic longitudinal velocity of the flow in the SOL and $D = \frac{\chi_e \chi_i}{\chi_e + \chi_i}$. Numerical analysis shows that these boundary conditions could be used to reproduce the evolution of edge temperature in L-mode plasma. The problem arises when we tried to use formulae (4-5) for the modelling of H mode discharges. It follows from numerical simulations that for these shots we can reproduce the experimentally observed ion and electron temperature near the separatrix only if we assume that perpendicular transport inside the transport barrier and in the SOL is of the order of neo-classical one. A similar conclusion has been recently derived from the analysis of H-mode density and temperature profiles near the separatrix in DIII-D [13]. Equations (4-5) need to be modified in this case because the formally defined SOL width $\Delta \propto \sqrt{D L_{||}/c_{SOL}}$ becomes less than the ion banana width. We use the simplest assumption that the only mechanism of ion flow through the separatrix is the direct losses of the banana ions [14,15] which leads to the following boundary conditions for ion's heat and particle flows:

$$\chi_i n_i \nabla T_i + \frac{3}{2} T_i D \nabla n_i \approx -n_i T_i \frac{\rho_{pi}}{\sqrt{\varepsilon}\tau_{ii}} F_T \quad (6)$$

$$D \nabla n_i \approx -\frac{n_i \rho_{pi}}{\sqrt{\varepsilon}\tau_{ii}} F_n \quad (7)$$

where ρ_{pi} – ion poloidal Larmor radius, τ_{ii} - ion-ion collisional frequency, ε– inverse aspect ratio near the separatrix. F_T and F_n are the coefficients which depend on the geometry, collisionality and radial electric field and $0 \le F_T, F_n \le 1$ [16,17]. The boundary condition for the electron heat flow is similar to (6) if we assume that the remaining magnetic turbulence near the separatrix keeps the electron's particle flux at the level of the ion neo-classical flow (7).

Before proceeding to the discussion of the result of numerical simulation, it is worth mentioning one interesting feature of boundary condition (6). Namely it follows from (6) that in the banana regime ion and electron heat flows do not depend on the temperature near the separatrix $Q_{e,i} \propto n_i n_{e,i}$. This feature allows us to explain the above mentioned experimentally

observed fact that the global plasma energy confinement time in hot-ion VH modes, formally defined as $\tau_E = W/(P_{tot} - dW/dt)$ grows almost linearly with time together with the total energy content W. From the point of view of the boundary condition (6) such a behaviour is a simple reflection of the fact that neo-classical losses at constant density do not depend on plasma energy and therefore do not provide a steady state solution of the energy balance equation. This statement can be clarified for the simplest situation of a slab plasma with uniform density $n=n_0=const$, thermal conductivity $\chi = \chi_0 = const$ and heating power deposition profile $p=p_0=const$. The solution of the energy balance equation

$$\frac{3}{2} n_0 \frac{\partial T}{\partial t} = p_0 + \frac{\partial}{\partial x} n_0 \chi_0 \frac{\partial T}{\partial x} \tag{8}$$

with the boundary condition (6) $\left(\chi_0 n_0 \nabla T\big|_{\rho=1} = -\beta n_0^2\big|_{\rho=1},\ \beta = const \right)$ could be found directly:

$$n_0 T(x.t) = \left(p_0 - \beta n_0^2/a\right)t + \frac{\beta n_0^2 a}{2\chi_0}\left(1 - \frac{x^2}{a^2}\right) \tag{9}$$

The first term in the right hand side of (9) describes the evolution of the temperature pedestal- it grows in time when the edge density is constant and there are no other mechanisms of energy losses (like radiation). The second term in the right hand side of (9) describes the radial profile. If we substitute the solution (9) into the definition of the energy confinement time τ_E we find:

$$\tau_E = \frac{a^2}{3\chi_0} + \frac{\left(p_0 - \beta n_0^2/a\right) \cdot t \cdot a}{\beta n_0^2} \tag{10}$$

It follows directly from (10) that the neo-classical boundary condition leads to the appearance of a non diffusive continuously growing term in the global energy confinement time.

We repeated the numerical simulations using the boundary condition (6) to predict edge temperatures. The results of this analysis allow us to reproduce the experimental observations for hot-ion VH mode shots on the evolution of temperature pedestal and the rise of thermal energy without saturation. This confirms our conclusion about the similarity of ELM-free JET H-mode discharges from the point of view of transport coefficients in the bulk plasma and shows the importance of the transport barrier near the separatrix.

To investigate the effect of enhanced radiation we have repeated the simulation of shot #26087 artificially imposing radiation losses increasing linearly in time up to 7MW. This prevents the formation of a high temperature pedestal and decreases the thermal energy rise. Fig.8 shows the experimental temporal evolution of the thermal energy for shot #26087

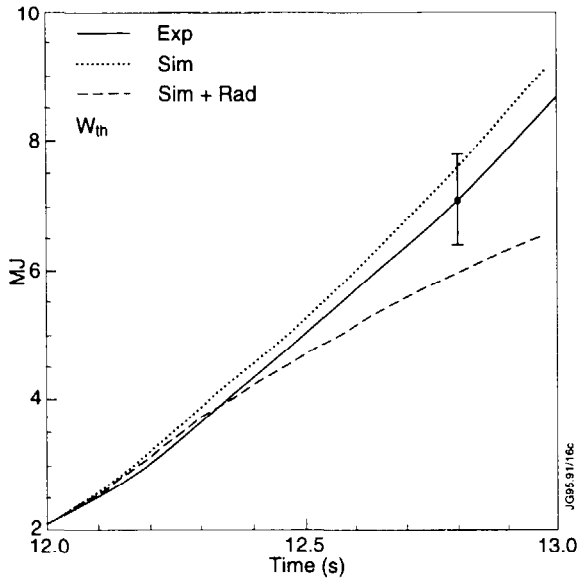

Fig.8: Time evolution of the thermal energy for simulations of shot #26087 using neo-classical boundary conditions

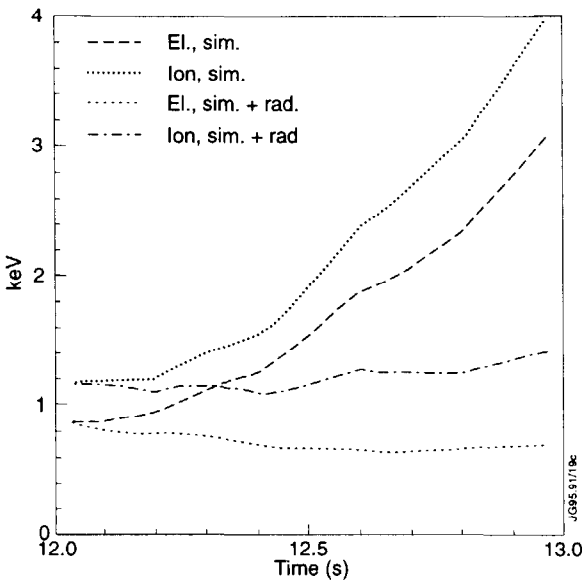

Fig.9: Edge ion and electron temperature time evolution (#26087).

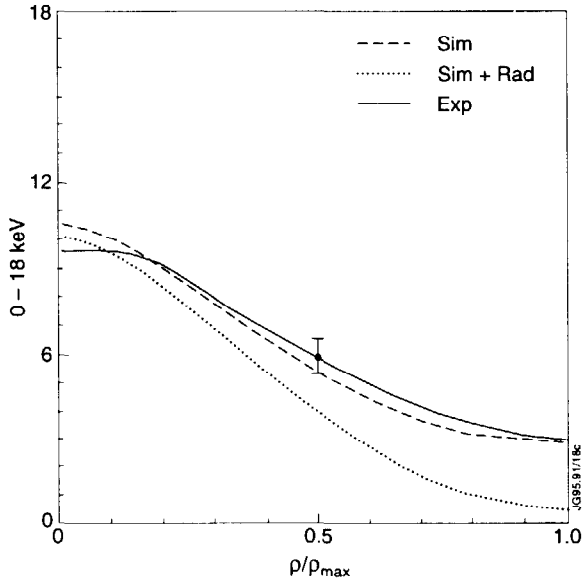

Fig.10 (a): Ion temperature profiles at t=12s and t=13s (#26087):

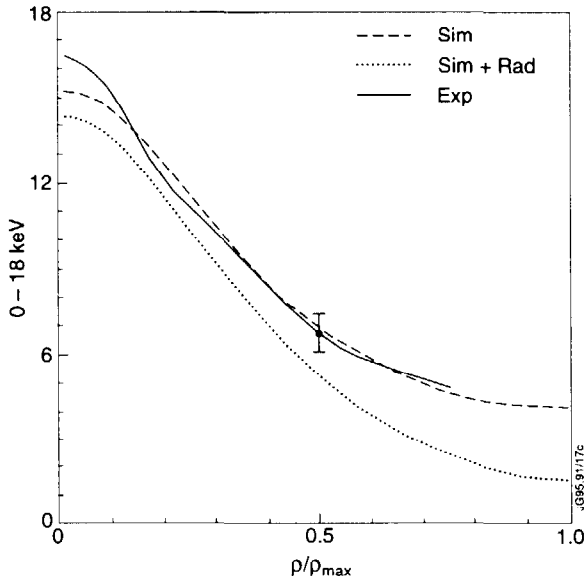

Fig.10 (b): Electron temperature profiles, traces as in Fig.10 (a).

together with the simulated values, obtained with or without the enhanced radiation. The time evolution of edge temperature is shown in Fig.9: the effect of radiation is clearly seen. In Fig.10a,b we show the characteristic radial profile for T_e and T_i for the same simulations and compared with experiment. Qualitatively the role of plasma convection is similar to the role of radiation. However correct self consistent treatment of plasma convection requires

simultaneous numerical simulation of both temperatures and densities. The results of such an analysis will be presented elsewhere.

IV. MODELLING OF THE ELMS IN JET.

Giant ELMs give another interesting example of fast global modification of plasma transport properties in JET. Following the DIII-D definition [18] we will discuss here only type I ELMs which repetition frequency increases with the heating power and which lead to a significant reduction in plasma performance.

The characteristic evolution of electron temperature during successive giant ELMs measured by the new 48 channels heterodyne radiometer system is shown in Fig. 11, together with the D signal for shot #30592 (I_p = 2.5MA, B_t =2.8T, P_{in} = 13MW, $<n_e>=3.010^{19}p/m^3$). These measurements, combined with the soft X-ray measurements [19] indicate that JET giant ELMs have a global character- the electron temperature is changed during MHD event not only near the plasma edge but far inside plasma volume. The characteristic radial extent of T_e drop at the onset of the MHD event increases with ELM amplitude and reaches value of $\Delta R \geq 0.4m$. The characteristic delay time between the onset of the T_e drop near the edge and in the mid radius is less than the diagnostics resolution time $\Delta\tau \approx 1ms$ and cannot be explained by the conventional theory of heat pulse propagation. The ELM appears to be triggered by an MHD event, which is accompanied by the excitation of a broad band range of magnetic fluctuations (see Fig.12). This short MHD burst is followed by a relatively long (with $\Delta\tau_L \approx (10 \div 30)ms$) phase of enhanced transport, after which the plasma returns to a quiescent H-mode phase. This second part of giant ELM is accompanied by a broad band of density fluctuations with a spectrum which is similar to those in L-mode plasma. Figure 13 shows the data from the recently installed multi-channel O-mode reflectometry, spanning the frequency range 18-70GHz, corresponding to critical densities in the range $0.43\text{-}6.00x10^{19}m^{-3}$. These data indicate the relative increase in dB in the fluctuation level for each channel, spanning the outer 10cm of the edge plasma. In the

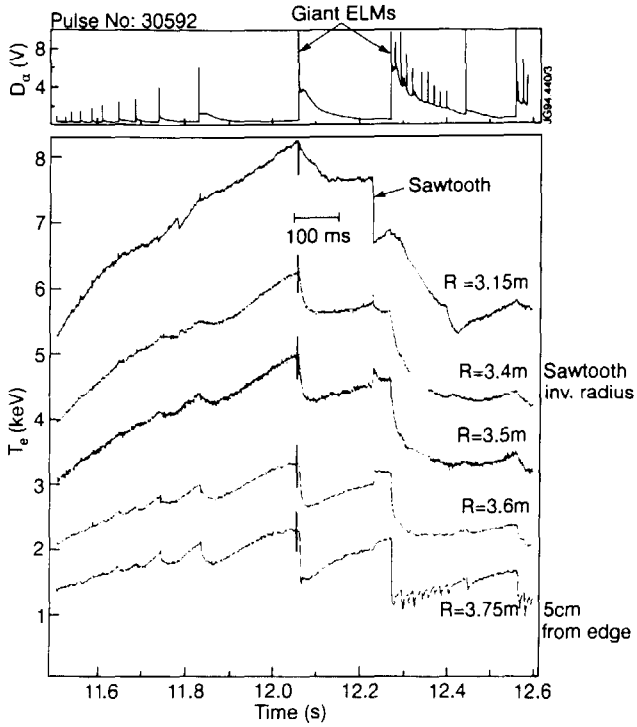

Fig.11: Time evolution of the D_α signal and of the electron temperature at different radial positions during giant ELMs in shot #30592.

outer channels, this increase is coincident with the rise of the D signal. In the innermost channels there is a delay of order 1ms.

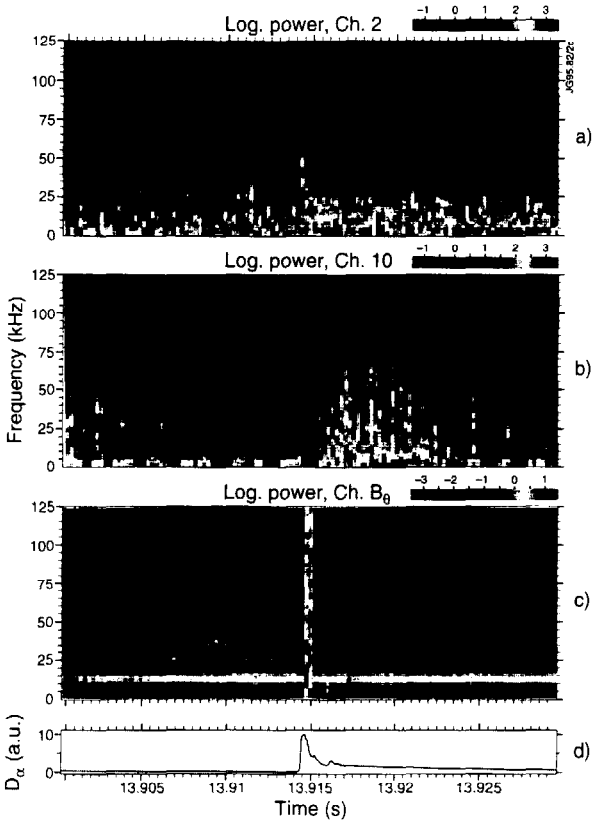

Fig.12: Broad-band activity, 10-125KHz, on reflectometer channels 1 to 10 covering a density range 0.43–6.00.10^{19}m^{-3} showing the instantaneous rise in the fluctuation level, coincident with the rise in the D_α signal which indicates the onset of a giant ELM.

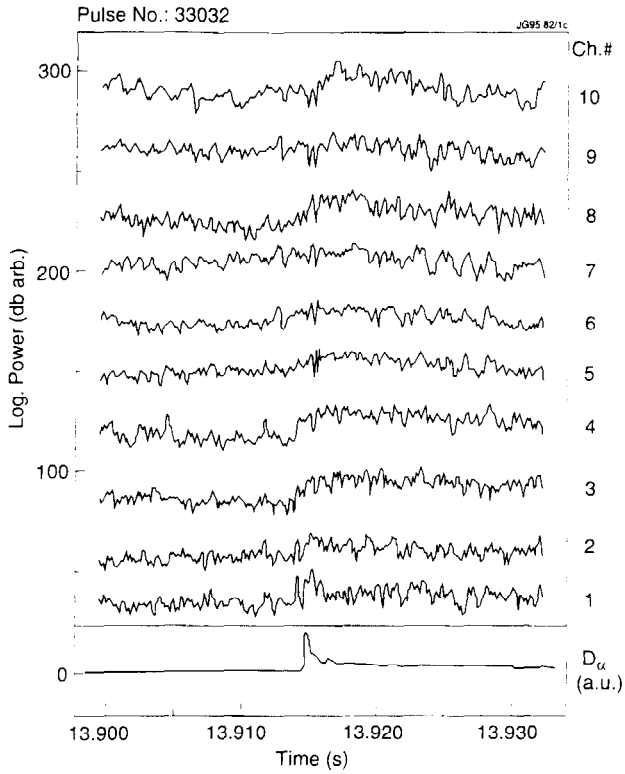

Fig.13: Time windowed power spectral analysis on a logarithmic colour scale of a) channel 2 (n=0.73.10^{19} m^{-3} and R≈3.87m), b) channel 10 (n=6.00.10^{19} m^{-3} and R≈3.77m) showing the different duration of the broad-band activity after the ELM and the delayed response for the innermost channel and c) Magnetic field fluctuations measured by a toroidal magnetic coil located at the top of the poloidal limiter.

Time windowed spectral analysis of density fluctuations during the giant ELM shows that the broad-band activity duration changes with radius (fig.12), from ~7ms in the innermost channel 10 (n=6.00x10^{19}m^{-3} and R3.77m) to at least 15ms in the outermost channel (n=0.4x10^{19}m^{-3} and R3.88m). The same behaviour is observed with E-mode reflectometry at 80GHz probing the edge of the plasma in similar discharges. Figure 12 also shows the 0.5ms burst of MHD activity at the start of the ELM. Two successive ELMs are separated by quiescent H mode phase which duration varies from ELM to ELM. Such a behaviour is similar to that found in DIII-D in the intermediate range of heating power and called compound ELM[18]. Compound ELMs in JET are quite regular when the heating power is well above the threshold of L-H transition.

We performed predictive numerical modelling of typical giant ELMs on JET keeping in mind the experimental observations. The main objective of this modelling were the following.

First of all we have checked whether transport coefficients during the second phase of compound ELMs indeed correspond to L-mode confinement. Hence we have tried modelling this phase with the Bohm model for L-mode given with the numerical coefficients (2).

Subsequently we have tried to find a transport model which reproduces the MHD events. In order to model this phase we adopt the following expression for the electron thermal diffusivity (we can only compare with experimental data for the electron temperature, and for the ions we simply use $\chi_i=3\chi_e$):

$$\chi_e^{MHD} = \chi_e^L\left(1+\alpha\cdot\exp\left(1-\rho/\Delta\rho\right)\right) \tag{12}$$

where χ_e^L is an electron thermal diffusivity in L-mode, is a numerical factor (varying from ELM to ELM, generally $\alpha\leq 10$), is the normalised radial coordinare ($\rho=1$ at the separatrix) and $\Delta\rho$– normalised radial width of the region with enhanced transport (usually $\Delta\rho\leq 0.2$-0.3). We point out that we are not proposing equation. (12) as a model for the MHD event: we use this expression empirically in order to follow the experimental temperature evolution and it might very well be that the temperature modification during the MHD event is not due to a diffusive process. However from the use of model (12) we will deduce the radial width of the MHD event $\Delta\rho$ and we will be able to evaluate the impact of the MHD event on the global confinement time.

The result of the modelling of two giant ELMs is shown in Figs. 14 and 15: as can be seen, the L-mode phase is necessary in order to obtain good agreement with the data. For these simulations we have used $\alpha=5$ for the ELM at t=51.82s and $\alpha=12.5$ for the ELM at t=52.06s;in both cases $\Delta\rho=20$cm has been used. Similar results have been obtained for the giant ELM of discharge 33032 at time t=53.915s, using $\alpha=10$, $\Delta\rho=20$cm for the MHD event.

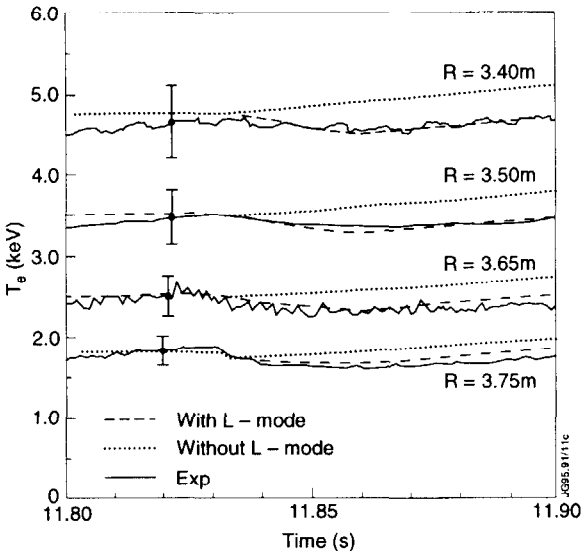

Fig.14: Time evolution of the experimental electron temperature at different radial positions during the giant ELM of #30592 at t=11.83s. The dotted lines represent the result of modelling these ELMs with and without a phase of L-mode-like transport after the initial MHD phase.

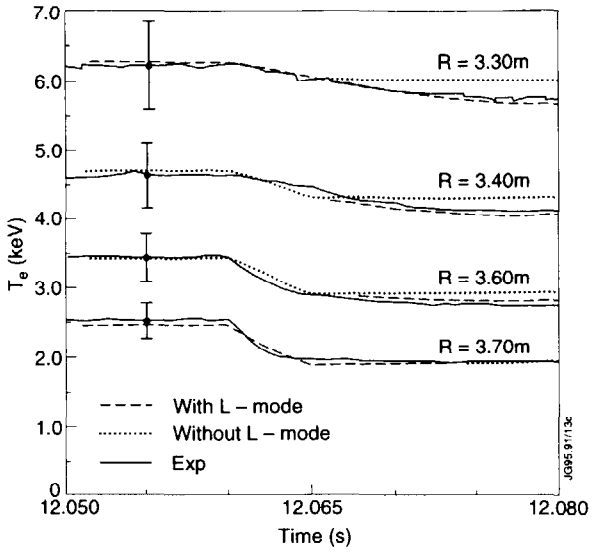

Fig.15: Time evolution of the experimental electron temperature at different radial positions during the giant ELM of #30592 at t=12.06s. The dotted lines represent the result of modelling these ELMs with and without a phase of L-mode-like transport after the initial MHD phase.

From our simulations we can also deduce information on the relative importance of the various phases in determining the global energy confinement time of ELMy H-mode JET plasmas. In order to proceed in this way, we have to define a proper time average of the energy confinement time for ELMy H-mode plasma $\langle \tau_E^{th} \rangle$:

$$\frac{1}{\langle \tau_E^{th} \rangle} = \frac{1}{\Delta t_\Sigma} \left(\frac{\Delta t_{MHD}}{\tau_E^{MHD}} + \frac{\Delta t_L}{\tau_E^L} + \frac{\Delta t_H}{\tau_E^H} \right) \tag{11}$$

where τ_E^{MHD}, τ_E^L, and τ_E^H are the computed energy confinement time during MHD , L-mode and H-mode phases of the compound ELM respectively and Δt_{MHD}, Δt_L, and Δt_H - the characteristic duration of these phases. The characteristic energy confinement times are computed under the assumption of a small relative variation of the total energy content by using the definition $\frac{1}{\tau_E^\alpha} \approx \frac{P - \frac{dW}{dt}_a}{W}$. For further discussion it is convenient to introduce the enhancement factor $H_\chi \equiv \langle \tau_E^{th} \rangle / \tau_E^{ITER89-L}$ which shows how much an effective energy confinement time in ELMy H mode exceeds the level of L-mode confinement. The main characteristic of plasma confinement for three successive ELMs for shot #30592, discussed earlier a compound ELM for shot #33032 and for cluster of small ELMs from shot #32386 are

Table 2.

shot	Δt_{MHD} (ms)	$\tau_E^{MHD}(s)$	$\Delta t_L(ms)$	$\tau_E^L(s)$	$\Delta t_H(ms)$	$\tau_E^H(s)$	$\frac{\Delta t_{MHD}\cdot\tau_E^L}{\tau_E^{MHD}\cdot\Delta t_L}$	$\langle\tau_E\rangle(s)$	H
#32386	2	0.09	-	-	5	1.7		0.28	1.3
#33032	2	0.04	40	0.41	80	2.3	0.5	0.67	1.8
#30592 large	3	0.04	30	0.18	130	1.1	0.45	0.45	2.1
#30592 medium	3	0.06	30	0.2	180	1.15	0.33	0.6	2.8
#30592 small	2	0.06	20	0.2	70	1.3	0.33	0.49	2.3

listed in Table 2. From this table the relative importance of the various phases of ELMs in determining of the time average electron thermal conductivity of ELMy H-mode JET plasma can be deduced (for example the parameter $\frac{\Delta t_{MHD}\cdot\tau_E^L}{\tau_E^{MHD}\cdot\Delta t_L}$ in Table 2 shows the relative importance of the MHD phase). It follows from our analysis that in the case of giant ELMs (discharges ##30592, 33032) the L-mode phases is the most important one in determining the global confinement, while the MHD event is less important due to its short duration. The picture is different for the cluster ELM of discharge #32386- the L-mode is absent in this case and the MHD event has a duration comparable to that of the H-mode phase (Fig.16). The resultant enhancement factor is slightly above L-mode (H=1.3). The results of numerical simulation of this ELM is shown on fig.17,18.

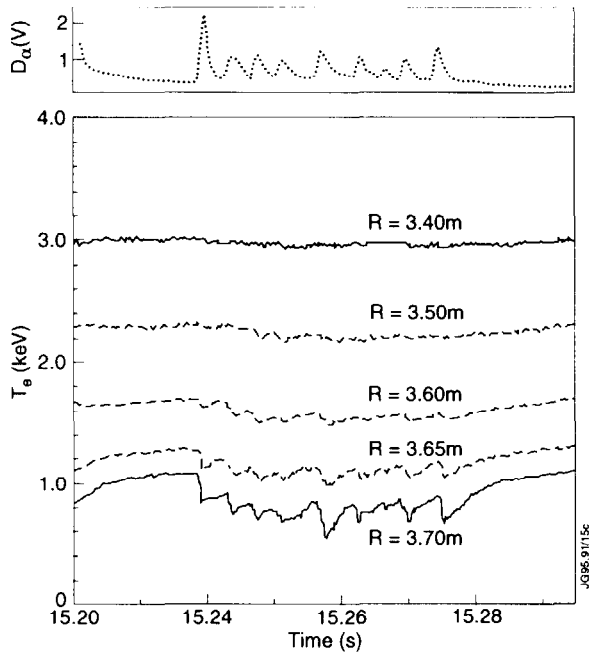

Fig.16: Time evolution of the D_α signal and of the experimental electron temperature at different radial positions during the "cluster" ELM of discharge 32386.

This result proves that a wide range of enhancement factor (1.3<H<2.8) can be brought about by ELMs with different characteristics.

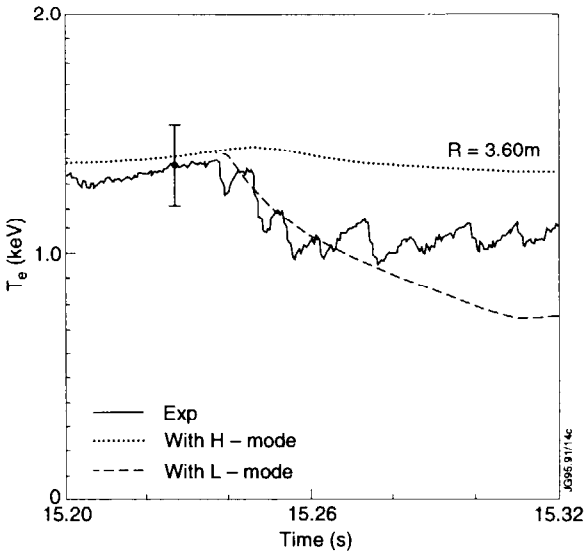

Fig.17: Time evolution of the experimental electron temperature at R=3.60 during the "cluster" ELM of discharge #32386, compared with the evolution resulting from the models for the L-mode and H-mode.

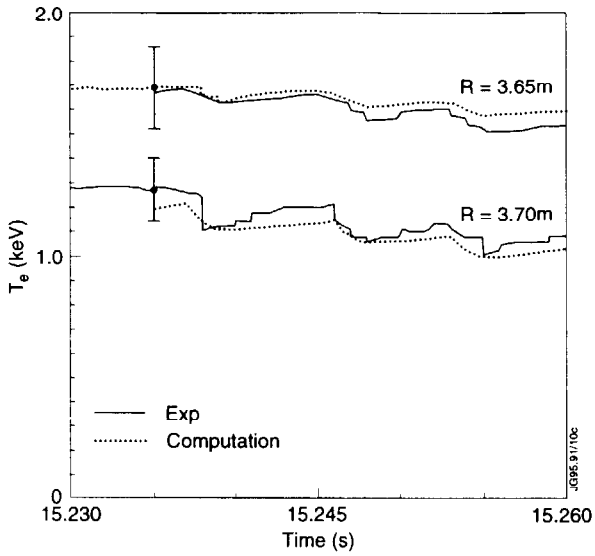

Fig.18: Time evolution of the experimental electron temperature at R=3.65, 3.70, during the "cluster" ELM in discharge #32386, compared with the results of the modelling of 3 successive ELMs with no L-mode-like phase.

CONCLUSIONS.

The numerical study of a series of ELM free JET shots with a wide range of plasma parameters allows us to conclude that within experimental accuracy discharges which have no sign of degradation of confinement due to MHD activity can be reproduced with the same transport model. The main differences between discharges with different enhancement factor $H \equiv \frac{\tau_E}{\tau_E^{ITER89}}$ lie not in the transport coefficients in the bulk plasma but in the variation of the transport barrier, different magnitude of impurity radiation, variation in the plasma convection and power deposition profile. This modelling confirms that the L-H transition can be described as a reduction of all transport coefficients everywhere outside q=1 surface immediately following the formation of the transport barrier near the separatrix. We have also shown that the formation of a large temperature pedestal just inside the separatrix in the case of hot ion H-modes can be simulated assuming that energy transport at the boundary reduces to that related to the direct losses of banana ions. The energy content related to such a pedestal is an important fraction of the total energy content and its time evolution explains the continuous increase of the enhancement factor H observed in these shots.

Finally an experimental study and transport analysis of giant ELMs in JET revealed that such ELMs have a composite structure - each of them is triggered by short MHD event which modify electron temperature not only near plasma edge but also far inside plasma volume. This short MHD event turns into much longer phase of enhanced transport that could be modelled as

an L-mode. A quiescent H-mode phase then follows. Therefore the ELMy H-mode plasma in JET (in cases when type I ELMs are dominant) is a composition of three different phases: short (with $\tau_{MHD} \approx 1ms$) MHD with transport coefficients much larger that in L-mode plasma, longer (with $\tau_L \approx 10-30ms$) phase of enhanced transport during which transport corresponds to L-mode confinement and finally ELM-free H-mode phase. The relative importance of each phase depends on the amplitude of the ELM with the general trend that relative importance of L-mode phase grows with ELM amplitude.

ACKNOWLEDGEMENTS.

The authors would like to acknowledge fruitful discussions with R. Giannella, T. Jones, J. Lingertat, P. Lomas, F. Nave, P. Thomas and K. Thomsen and Task Force H and D for providing the experimental information.

REFERENCES.

[1] Cordey, J.G., Muir, D.G., Neudachin, S.V., Parail, V.V., et al., Plasma Physics and Contr. Fusion, **36**, A267, (1994),

[2] Becker, G., Murmann, H.D., Nucl. Fusion **28** (1988) 2179.

[3] Kurki-Suonio, T.K., et al., Nucl. Fusion **33** (1993) 301.

[4] Connor, J.W., Hastie, R.J., and Taylor, J.B. Proc. Roy. Soc. London Ser. A 365, 1 (1979),

[5] Cenacci G., Taroni A., "JETTO: A Free-Boundary Plasma Transport Code", Rapporto ENEA RT/TIB 88(5) 1988.

[6] The JET Team, 15th Int. Conf. on Plasma Physics and Contr. Nuclear Fusion Research, Seville, Spain 1994, CN-60/A-2-I-4.

[7] Z. Chang et.al., Nucl. Fus.**31** (1991) 1309.

[8] Sesnic S., et al., Plasma Physics and Control. Fusion **36** (1994) A225.

[9] Park, H.K., et al., Nuclear Fusion, **32**, (1992), 1042.

[10] Cordey, J.G., et al., Nuclear Fusion **35**, (1995), 101.

[11] Taroni, A., Erba, M., Springmann, E. and Tibone, F., Plasma Physics and Contr. Fusion, **36**, (1994), 1629.

[12] Parail V.V. et al., 15th Int. Conf. on Plasma Physics and Contr. Nuclear Fusion Research, Seville, Spain 1994, CN-60/A-2-II-3.

[13] Mandl, W., et al., Nuclear Fusion **35**, (1995), 347.

[14] Hinton, F.L., Nuclear Fusion **25**, (1985), 1457.

[15] Weisen H., et al., Nuclear Fusion **31**, (1991), 2247.

[16] S.-I. Itoh and K. Itoh, Phys. Rev. Letters, **60**, (1988), 2276.

[17] Shaing K.C. and E.C. Crume,Jr., Phys. Fluids, **63**, (1989), 2369.

[18] Schissel, D.P, et al., Proc. 19th European Conference on Controlled Fusion and Plasma Physics, Innsbruck, Austria, 1992, Vol. I, p. 235.

[19] M.F.F. Nave et al., Proc. 1994 International Conference on Plasma Physics, Foz do Iguaci, Parana, Brazil, 1994, also JET-P(95), 03.